Modeling light-driven proton pumps in artificial photosynthetic reaction centers

Pulak Kumar Ghosh,[1] Anatoly Yu. Smirnov,[1,2] and Franco Nori[1,2,a)]
[1]*Advanced Science Institute, The Institute of Physical and Chemical Research (RIKEN), Wako-shi, Saitama 351-0198, Japan*
[2]*Department of Physics, Center for Theoretical Physics, University of Michigan, Ann Arbor, Michigan 48109-1040, USA*

(Received 2 April 2009; accepted 12 June 2009; published online 17 July 2009)

We study a model of a light-induced proton pump in artificial reaction centers. The model contains a molecular triad with four electron states (i.e., one donor state, two photosensitive group states, and one acceptor state) as well as a molecular shuttle having one electron and one proton-binding sites. The shuttle diffuses between the sides of the membrane and translocates protons energetically uphill: from the negative side to the positive side of the membrane, harnessing for this purpose the energy of the electron-charge separation produced by light. Using the methods of quantum transport theory we calculate the range of light intensity and transmembrane potentials that maximize both the light-induced proton current and the energy transduction efficiency. We also study the effect of temperature on proton pumping. The light-induced proton pump in our model gives a quantum yield of proton translocation of about 55%. Thus, our results explain previous experiments on these artificial photosynthetic reaction centers. © *2009 American Institute of Physics*.
[DOI: 10.1063/1.3170939]

I. INTRODUCTION

It would be desirable to create an artificial system that exploits the basic principles of natural photosynthesis in order to produce energy in an usable form.[1–7] Indeed, natural photosynthetic structures efficiently convert the energy of light into chemical form.[7,8]

The overall energy transduction process in plant photosynthesis occurs through a number of strongly coupled successive stages (see, e.g., Refs. 1, 2, and 8). In the first step, the light of the appropriate wavelength is absorbed by a light harvesting complex. The second step involves the conversion of electronic excitation energy to redox potential in the form of the long-lived transmembrane charge separation via multistep electron transfer processes. The first two steps involve three constituents: (a) light-absorbing pigments, (b) an electron acceptor, and (c) an electron donor. In the third step, the energy stored in the electron subsystem is used for energetically uphill proton pumping, which generates the proton motive force across the membrane.

The study of natural photosynthesis has inspired researchers to perform the photoinduced energy transduction processes in the laboratory.[1–7,9–12] A convenient approach to photosynthesis in artificial reaction centers is to use synthetic pigments, electron acceptors, and electron donors that are very similar in molecular structure to natural pigments (e.g., chlorophylls, carotenoids, and quinones). In this direction, the experimental model proposed in Refs. 9 and 10 provides a paradigm for the conversion of light energy to a proton potential gradient. These seminal works[9,10] have motivated research in the design and synthesis of new artificial photosynthetic systems[13–15] (i.e., light-harvesting antennas and reaction centers) and triggered considerable experimental[16–20] and theoretical[21–24] activities to investigate more sophisticated and more efficient mechanisms for the conversion of light energy.

The transformation of light energy into the electrochemical gradient of protons across the membrane can be quantitatively characterized by the quantum yield (or quantum efficiency) Φ of proton translocation. This parameter is defined as the total number of translocated protons divided by the number of photons absorbed by the triad.[9] A quantum yield of the order of 0.4% has been measured in Ref. 9. A much higher quantum efficiency $\Phi \sim 7\%$ for the conversion of photons into adenosine triphosphate (ATP) molecules was found in Ref. 10. As argued in Ref. 10, the actual quantum yield of ATP formation could be of the order of 15% if we take into account the real rate of light absorbance, which is $\sim 50\%$. Near four protons are necessary for the synthesis of a single ATP molecule. This means that the real quantum yield Φ of proton translocation measured in Ref. 10 can be about 60%. The total thermodynamic (or power-conversion) efficiency η of the light-to-ATP conversion process is estimated in Ref. 10 as $\eta \sim 4\%$.

In the present paper, using methods from quantum transport theory,[25–28] we analyze the photoinduced electron and proton transfer in a molecular triad inserted into a liposomal membrane, which contains a single molecular shuttle. We calculate the photon-to-proton quantum yield $\Phi \sim 55\%$ (and the thermodynamic efficiency $\eta \sim 6.3\%$) for the resonant tunneling conditions when the reorganization energy λ of the electron transitions matches the detuning δ between the electron energy levels: $\lambda \sim \delta$.

We note that due to a small optimal value of the reorga-

a)Electronic mail: fnori@riken.jp.

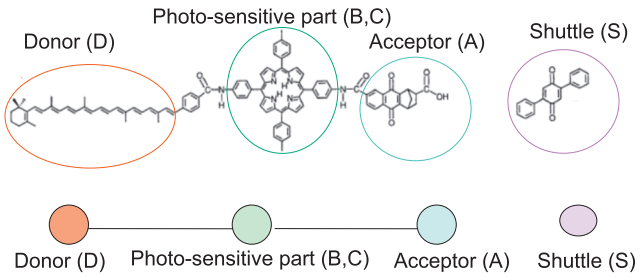

FIG. 1. The top figure presents the triad (donor D, photosensitive part B,C, and acceptor A) and the shuttle S (Refs. 9 and 10). These are enclosed by color circles, which are schematically shown in the bottom figure. The tetraarylporphyrin group acts as a photosensitive moiety (B,C) (inside the green circle in the top structure). This is connected to both a naphthoquinone moiety fused to a norbornene system with a carboxylic acid group [which acts as an electron acceptor (A)] and to a carotenoid polyene [which acts as an electron donor (D)]. 2,5-diphenylbenzoquinone is the proton shuttle (S) denoted by a pink hollow circle in the structure and by a solid pink circle in the cartoon.

nization energy ($\lambda \sim 400$ meV) the charged recombination process in the triad is described by the inverted region of the Marcus formula.[29–31] This further enhances the performance of the system. Our results explain the experiments made in Ref. 10 using artificial photosynthetic centers. The obtained power-conversion efficiency corresponds to the highest value $\eta \sim 6.5\%$ achieved recently with polymer solar cells.[32] It is expected that the proton current and the efficiency should increase with increasing the number of the shuttles in the membrane.

This article is organized as follows. In Sec. II (see also the Appendix) we introduce the basis set for the system and write the Hamiltonian of the problem. In Sec. III, we present the master equation for the density matrix coupled to the Langevin equation describing the diffusive motion of the shuttle in the lipid bilayer. In Sec. IV, we numerically solve these equations and analyze the light-induced proton pumping process. In Sec. V we summarize our results.

II. MODEL

We use a slightly modified version of the well-accepted model already presented, e.g., in Refs. 9 and 10. In this model the reaction center is a molecular triad containing an electron donor and an electron acceptor both linked to a photosensitive porphyrin group (shown in Fig. 1). The triad molecule (D-BC-A) is inside the bilayer of a liposome. The lipid bilayer also contains freely diffusing 2,5 diphenylbenzoquinones acting as proton shuttles. The molecular triad absorbing a photon establishes a negative charge near the outer surface and a positive charge near the inner surface of the liposome by generating charge separated species D^+-BC-A^-. The freely diffusing quinone shuttle translocates an electron-proton pair across the membrane and neutralizes the molecular triads.

In Fig. 2 we schematically illustrate the process of light-induced proton pumping in liposomes by artificial photosynthetic reaction centers.[9,10] The transmembrane proton pumping requires a symmetric arrangement of the molecular triad (length of ~ 8 nm) inside the bilayer and with a specific direction: with the acceptor (A) site toward the outer membrane of the liposome [the negative (N) side of the membrane] and with the donor (D) toward the inside of the liposome [the positive (P) side of the membrane].[9,10]

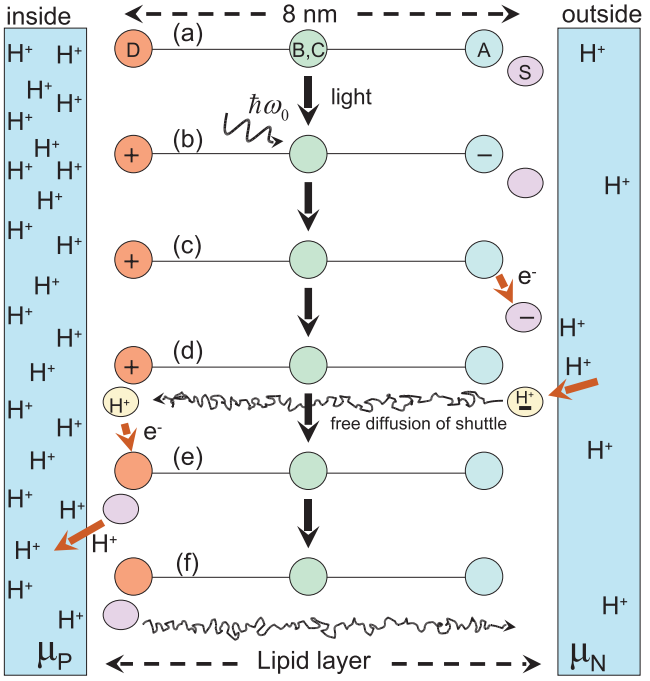

FIG. 2. Schematic diagram of the light-induced proton pump across the lipid bilayer in a liposomic membrane. A molecular triad D-BC-C is symmetrically inserted in the lipid bilayer. The different stages in the proton pumping process are here denoted by (a), (b), (c), (d), (e), and (f). The two bluish vertical rectangles on both sides schematically represent two proton reservoirs with electrochemical potentials μ_P and μ_N. These two proton reservoirs correspond to the aqueous phases inside and outside of the liposome, respectively. The shuttle molecule S is shown as a pink-colored oval and the protonated neutral shuttle is shown as a yellow oval. This shuttle freely diffuses in (d) (the black scribbled curves represent the thermal stochastic motion of the shuttle) across the membrane to transport a proton from the lower proton potential μ_N to the higher proton potential μ_P side of the membrane, where $(\mu_P - \mu_N)$ denotes the total potential difference between the two reservoirs.

The energy diagrams of the electron and proton sites are shown in Figs. 3 and 4. There are two electrons in the system, one of which is initially on the D site and another electron is on the lower energy level B. The quinone molecular shuttle has one electron state S (denoted by S instead of S_e) and one proton state Q (denoted here by Q instead of S_p). Thus, S denotes the shuttle electron state and Q denotes the shuttle proton state.

The overall process leading to the proton translocation from the N-reservoir with a lower proton potential μ_N to the P-reservoir with a *higher* electrochemical potential μ_P can be considered as a sequence of eight stages (most of which are shown in Fig. 2).

- Step I: The photosensitive moiety of the molecular triad absorbs light and an electron goes from the ground state B to the excited state C [see Fig. 3(b)].
- Step II: The unstable excited state C transfers the electron to the acceptor A, producing an unstable charge-separated intermediate species D-BC^+-A^-.
- Step III: The unstable intermediate charge-separated

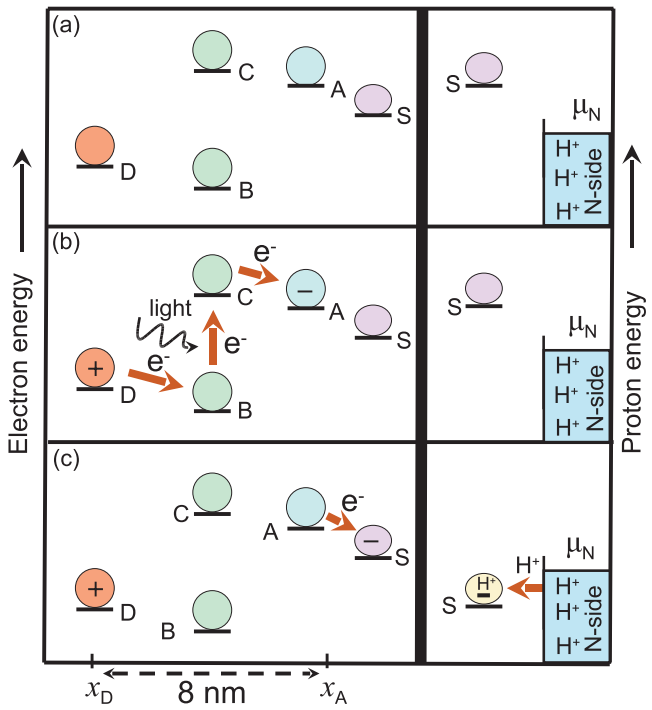

FIG. 3. Energy diagram depicting the energy levels of states involved in an artificial photosynthetic reaction center *before* the diffusion of the shuttle to the *P*-reservoir. (a)–(c) correspond to the stages (a), (b), and (c) in Fig. 2. The left and right panels represent electron and proton energy levels, respectively. The abbreviations *D*, *B*, *C*, *A*, and *S* are the same as used in the text and in Fig. 1. Also, x_D and x_A represent the spatial coordinates of sites *D* and *A*, respectively. The thick brown arrows denote the path the electrons follow in this energy diagram, generating charge separation in (b) and shuttle charging and protonation in (c). Initially, light excites an electron from *B* to *C* and eventually to *A*, making it A^-. Afterward, in (b), the donor *D* loses an electron, thus becoming D^+, and that electron moves to *BC*. Later on, the shuttle *S* in (c) receives the electron from *A*.

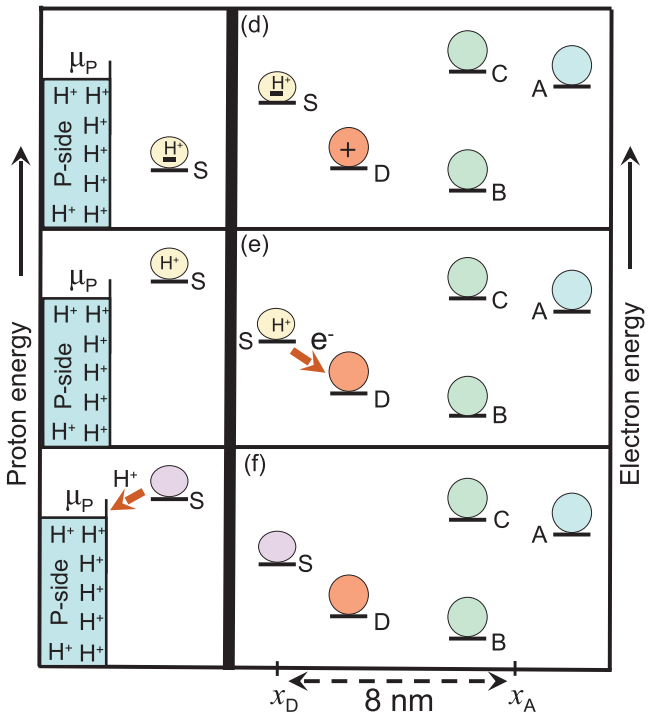

FIG. 4. Energy levels involved in an artificial photosynthetic reaction center. This figure is similar to Fig. 3, but now the energy profile corresponds to the stage *after* the shuttle diffuses to the *P*-reservoir. Here (d)–(f) correspond to the stages (d), (e), and (f) in Fig. 2. The left and right panels represent proton and electron energy levels, respectively. The thick brown arrows denote the path followed by the (e) electron and (f) proton. In (d), an electron on the shuttle *S* moves to the donor site *D*, neutralizing it in (e). This electron transition in the right panels increases the proton energy of the shuttle, as shown in the left panels [(d) and (e)]. The proton finally leaves the shuttle in the left panel of (f).

species is rapidly rearranged to a relatively stable charge-separated form (D^+-*BC*-A^-) by the thermal electron transfer from the state *D* to the state B^+ having a lower energy than the state *D* [Fig. 3(b)].

- Step IV: The shuttle in the position near the *N*-side of the membrane accepts an electron from A^- and becomes negatively charged.
- Step V: The shuttle molecule receives a proton from the *N*-reservoir and becomes neutralized [Fig. 3(c) right panel].
- Step VI: The neutral shuttle slowly diffuses through the lipid bilayer and carries the electron and the proton to the *P*-side of the membrane and to the *D*-site [stage (d) in Fig. 2].
- Step VII: The shuttle gives away the electron to the positively charged site D^+ [stage (e) in Fig. 2 and Fig. 4(e)].
- Step VIII: The shuttle is deprotonated by donating the proton to the *P*-reservoir [Fig. 4(f)].

This sequence of eight steps describes the photoinduced electron transfer that generates the intramembrane redox potential, which in turn drives the energetically uphill vectorial translocation of protons by the shuttle. Electrons in the state i $(=D,B,C,A,S)$ and protons in the state Q are characterized by the corresponding Fermi operators a_i^+, a_i and b_Q^+, b_Q with the electron population operator n_i and the proton population n_Q. We assume that each electron or proton state can be occupied by a single electron or a single proton. Spin degrees of freedom are neglected. The proton site on the shuttle denoted by Q can be populated from the *N*-reservoir provided the shuttle is within the transition length L_Q from the *N*-side of the membrane. The protonated shuttle located within the transition (or tunneling) range from the *P*-side of the membrane can donate its proton to the *P*-reservoir. Protons in the reservoirs are described by the Fermi operators $d_{k\alpha}^+, d_{k,\alpha}$, where $\alpha=N,P$, and k is an additional parameter which has the meaning of a wave vector in condensed matter physics.[25–28] The number of protons in the reservoirs is determined by the operator $\Sigma_k N_{k\alpha}$ with $N_{k\alpha}=d_{k\alpha}^+ d_{k\alpha}$.

A. Hamiltonian

The Hamiltonian of the electron-proton system

$$H = H_0 + H_{\mathrm{dir}} + H_{\mathrm{tr}} + H_B \tag{1}$$

has a term H_0 related to the energies E_i of the electron eigenstates $(i=D,B,C,A,S)$ and to the energy ϵ_Q of a proton on the shuttle

$$H_0 = \sum_i E_i n_i + \epsilon_Q n_Q + u_{DB}(1-n_D)(1-n_B-n_C) - u_{DA}(1-n_D)n_A - u_{BA}(1-n_B-n_C)n_A - u_{SQ}n_S n_Q. \quad (2)$$

We include here the electrostatic interaction between the electron sites u_{DB}, u_{DA}, u_{BA} and the Coulomb attraction u_{SQ} between the electron and proton sites on the shuttle. It is assumed that the empty donor state D (with $n_D=0$) as well as the empty photosensitive groups B and C ($n_B+n_C=0$) have positive charges and $u_{DB}=u_{DC}$, $u_{CA}=u_{BA}$.

The term

$$H_{\rm dir} = -\Delta_{DB}a_D^\dagger a_B - \Delta_{AC}a_A^\dagger a_C - \Delta_{DS}(x)a_D^\dagger a_S - \Delta_{AS}(x)a_A^\dagger a_S - F(t)a_B^\dagger a_C + \text{H.c.} \quad (3)$$

describes the tunneling of electrons between the sites D-B, C-A, A-S, and D-S with the corresponding amplitudes $\Delta_{ii'}$. Notice that the tunneling elements $\Delta_{DS}(x)$ and $\Delta_{AS}(x)$ depend on the shuttle position x. The Hamiltonian $H_{\rm dir}$ is also responsible for the electron transitions between the states B and C induced by the electromagnetic field (light) $F(t)=F_0\exp(i\omega_0 t)$ with a frequency ω_0 and an amplitude F_0. Proton transitions between the shuttle (site Q) and the N- and P-proton reservoirs are governed by the Hamiltonian

$$H_{\rm tr} = -\sum_{k\alpha} T_{k\alpha}(x)d_{k\alpha}^\dagger b_Q - \sum_{k\alpha} T_{k\alpha}^*(x)b_Q^\dagger d_{k\alpha} \quad (4)$$

with the position-dependent coefficients $T_{k\alpha}(x)$. We have chosen the following form of $T_{k\alpha}(x)$:

$$T_{kN}(x) = T_{kN}\theta[x-(x_N-L_Q)],$$

$$T_{kP}(x) = T_{kP}\theta[x_P+L_Q-x],$$

where $\theta(x)$ is the Heaviside step function and the parameter L_Q defines the proton loading range of the shuttle.

B. Interaction with the environment

To take into consideration the effect of a dissipative environment we consider the well-known system-reservoir model,[29,30,33] where the medium surrounding the active sites is represented by a system of harmonic oscillators with the Hamiltonian

$$H_B = \sum_j \left[\frac{p_j^2}{2m_j} + \frac{m_j\omega_j^2}{2}\left(x_j + \frac{1}{2}\sum_i x_{ji}n_i\right)^2\right], \quad (5)$$

where x_j, p_j are the positions and momenta of the oscillators with effective masses m_j and frequencies ω_j. The parameters x_{ji} determine the strengths of the coupling between the electron subsystem and the environment. The system of independent oscillators is conveniently characterized by the spectral functions $J_{ii'}(\omega)$ defined by

$$J_{ii'}(\omega) = \sum_j \frac{m_j\omega_j^3(x_{ji}-x_{ji'})^2}{2}\delta(\omega-\omega_j), \quad (6)$$

so that the reorganization energy $\lambda_{ii'}$ related to the $i\to i'$ transition has the form

$$\lambda_{ii'} = \int_0^\infty \frac{d\omega}{\omega}J_{ii'}(\omega) = \sum_j \frac{m_j\omega_j^2(x_{ji}-x_{ji'})^2}{2}. \quad (7)$$

With the unitary transformation $\hat{U}=\Pi_i\hat{U}_i$, where

$$\hat{U}_i = \exp\left[\frac{i}{2}\sum_j p_j x_{ji}n_i\right], \quad (8)$$

we can transform the Hamiltonian H to the form $H'=U^\dagger HU$ becoming (after dropping the prime)

$$H = H_0 - \sum_{ii'}\Delta_{ii'}e^{(i/2)(\xi_i-\xi_i')}a_{i'}^\dagger a_i - F(t)e^{-(i/2)(\xi_B-\xi_C)}a_B^\dagger a_C - F^*(t)a_C^\dagger a_B e^{(i/2)(\xi_B-\xi_C)} - \sum_{k\alpha}T_{k\alpha}(x)d_{k\alpha}^\dagger b_Q - \sum_{k\alpha}T_{k\alpha}^*(x)b_Q^\dagger d_{k\alpha} + \sum_j\left(\frac{p_j^2}{2m_j}+\frac{m_j\omega_j^2x_j^2}{2}\right), \quad (9)$$

where $\alpha=N,P$ and the tunneling coefficients $\Delta_{ii'}^*=\Delta_{i'i}$ take nonzero values only for transitions between the sites D and B, A and C, A and S, as well as D and S. The stochastic phase operator ξ_i is given by

$$\xi_i = \frac{1}{\hbar}\sum_j p_j x_{ji}. \quad (10)$$

The result of this transformation follows from the fact that for an arbitrary function $\Phi(x_j)$, the operator $\hat{U}$ produces a shift in the oscillator positions

$$\hat{U}^\dagger\Phi(x_j)\hat{U} = \Phi\left(x_j + \frac{1}{2}\sum_i x_{ji}n_i\right). \quad (11)$$

This transformation also results in the phase factors for the electron amplitudes [see Eq. (9)].

The basis sets composed of the electron-proton eigenstates and their corresponding energy eigenvalues are presented in the Appendix. Thus, the reader is encouraged to read this short Appendix before proceeding further.

III. TIME EVOLUTION OF DENSITY MATRIX

A. Master equations

To describe the time evolution of the diagonal elements of the density matrix $\langle\rho_m\rangle$, we write the Heisenberg equation for the operators ρ_m with the subsequent averaging over the environment fluctuations and over the states of the proton reservoirs,

$$\langle\dot{\rho}_m\rangle = -\langle i[\rho_m, H_{\rm dir}]_-\rangle - \langle i[\rho_m, H_{\rm tr}]_-\rangle. \quad (12)$$

The protons in the reservoirs ($\alpha=N,P$) are characterized by the Fermi distributions,

$$F_\alpha(E_{k\alpha}) = \left[\exp\left(\frac{E_{k\alpha}-\mu_\alpha}{T}\right)+1\right]^{-1} \quad (13)$$

with the temperature T ($k_B=1$). The electrochemical potentials μ_N and μ_P correspond to the negative (N) and positive (P) proton reservoirs, respectively. The proton motive force ($\Delta\mu$) across the membrane is given by

$$\Delta\mu = \mu_P - \mu_N = V - \frac{2.3RT}{F}(\Delta p\mathrm{H}), \tag{14}$$

where R and F are the gas constant and Faraday constant, respectively, and V is the transmembrane voltage gradient. Hereafter we change $\Delta\mu$ by changing the pH of the solution by ΔpH.

The contribution of the transitions between the shuttle and the proton reservoirs to the time evolution of the density matrix is described by the second term in the right hand side of Eq. (12), which can be calculated with methods of quantum transport theory[25,26]

$$\langle i[\rho_m, H_{\mathrm{tr}}]_-\rangle = \sum_n [\gamma^{\mathrm{tr}}_{nm}(x)\langle\rho_m\rangle - \gamma^{\mathrm{tr}}_{mn}(x)\langle\rho_n\rangle] \tag{15}$$

with the relaxation matrix

$$\gamma^{\mathrm{tr}}_{mn}(x) = \sum_\alpha \Gamma_\alpha(x)\{|b_{Q,mn}|^2[1 - F_\alpha(\omega_{nm})] + |b_{Q,nm}|^2 F_\alpha(\omega_{mn})\}. \tag{16}$$

Here we introduce the frequency-independent coefficients

$$\Gamma_\alpha(x) = 2\pi\sum_k |T_{k\alpha}(x)|^2\delta(\omega - E_{k\alpha}), \tag{17}$$

which determine the transition rates between the shuttle state Q and the sides of the membrane (N- and P-reservoirs). Notice that these coefficients are functions of the shuttle position x.

The transitions between the electron levels are described by the Hamiltonian H_{dir}, which can be written as

$$H_{\mathrm{dir}} = -\sum_{mn} \mathcal{A}_{mn}\rho_{m,n} - \sum_{mn} \rho_{n,m}\mathcal{A}^\dagger_{mn} \tag{18}$$

with the functions

$$\mathcal{A}_{mn} = Q_{DB}(a^\dagger_B a_D)_{mn} + Q_{CA}(a^\dagger_A a_C)_{mn} + Q_{SA}(a^\dagger_A a_S)_{mn} + Q_{SD}(a^\dagger_D a_S)_{mn} + Q_{CB}(a^\dagger_B a_C)_{mn}, \tag{19}$$

which are defined as superpositions of the heat-bath operators

$$Q_{ii'} = \Delta_{i'i}\exp[(i/2)(\xi_i - \xi_{i'})] = \Delta_{i'i}\exp\left[(i/2)\sum_j p_j(t)(x_{ji} - x_{ji'})\right] \tag{20}$$

for the pairs of the electron sites $(ii') = (DB), (CA), (SA), (SD)$, whereas for the pair (CB) we have

$$Q_{CB} = F_0\exp(i\omega_0 t)\exp\left[(i/2)\sum_j p_j(t)(x_{jC} - x_{jB})\right]. \tag{21}$$

In the case of a high-enough temperature of the bath,[30] the cumulant functions of the unperturbed operators $Q^{(0)}_{ii'}$ are determined by the relations

$$\langle Q^{(0)}_{ii'}(t), Q^{(0)\dagger}_{ii'}(t')\rangle = |\Delta_{i'i}|^2 e^{-i\lambda_{ii'}(t-t')}e^{-\lambda_{ii'}T(t-t')^2}, \tag{22}$$

$$\langle Q^{(0)\dagger}_{ii'}(t), Q^{(0)}_{ii'}(t)\rangle = |\Delta_{i'i}|^2 e^{i\lambda_{ii'}(t-t')}e^{-\lambda_{ii'}T(t-t')^2}.$$

The contribution of the electron transitions to Eq. (12) is determined by the term

$$\langle -i[\rho_m, H_{\mathrm{dir}}]_-\rangle = i\sum_n \langle \mathcal{A}_{mn}\rho_{mn} - \mathcal{A}_{nm}\rho_{nm}\rangle + \mathrm{H.c.} \tag{23}$$

Within the theory of open quantum systems developed in Ref. 28, the correlation function $\langle\mathcal{A}_{mn}\rho_{mn}\rangle$ is proportional to the density matrix elements of the system $\langle\rho_m\rangle$ with coefficients defined by the unperturbed correlators $\langle\mathcal{A}^{(0)}_{mn}(t), \mathcal{A}^{(0)\dagger}_{mn}(t')\rangle$ of the bath operators

$$\langle\mathcal{A}_{mn}(t)\rho_{mn}(t)\rangle = i\int dt_1\,\theta(t - t_1)e^{i\omega_{mn}(t-t_1)} \times\{\langle\mathcal{A}^{(0)}_{mn}(t), \mathcal{A}^{(0)\dagger}_{mn}(t_1)\rangle\langle\rho_m(t)\rangle - \langle\mathcal{A}^{(0)\dagger}_{mn}(t_1), \mathcal{A}^{(0)}_{mn}(t)\rangle\langle\rho_n(t)\rangle\}, \tag{24}$$

where

$$\begin{aligned}\langle\mathcal{A}^{(0)}_{mn}(t), \mathcal{A}^{(0)\dagger}_{mn}(t_1)\rangle = {}& \langle Q^{(0)}_{CB}(t), Q^{(0)\dagger}_{CB}(t_1)\rangle|(a^\dagger_B a_C)_{mn}|^2 \\ &+ \langle Q^{(0)}_{DB}(t), Q^{(0)\dagger}_{DB}(t_1)\rangle|(a^\dagger_B a_D)_{mn}|^2 \\ &+ \langle Q^{(0)}_{CA}(t), Q^{(0)\dagger}_{CA}(t_1)\rangle|(a^\dagger_A a_C)_{mn}|^2 \\ &+ \langle Q^{(0)}_{SA}(t), Q^{(0)\dagger}_{SA}(t_1)\rangle|(a^\dagger_A a_S)_{mn}|^2 \\ &+ \langle Q^{(0)}_{SD}(t), Q^{(0)\dagger}_{SD}(t_1)\rangle|(a^\dagger_D a_S)_{mn}|^2\end{aligned} \tag{25}$$

and the reverse expression can be obtained for the correlator $\langle\mathcal{A}^{(0)\dagger}_{mn}(t_1), \mathcal{A}^{(0)}_{mn}(t)\rangle$. The formula (24) is valid in the case of weak tunneling and weak driving force F_0. The effects of quantum coherence are also neglected here.

Finally, we derive the master equation for the density matrix of the system

$$\langle\dot\rho_m\rangle + \sum_n \gamma_{nm}(x)\langle\rho_m\rangle = \sum_n \gamma_{mn}(x)\langle\rho_n\rangle \tag{26}$$

with the total relaxation matrix

$$\gamma_{mn}(x) = \gamma^{\mathrm{tr}}_{mn}(x) + (\kappa_{DB})_{mn} + (\kappa_{CA})_{mn} + (\kappa_{SA})_{mn} + (\kappa_{SD})_{mn} + (\kappa_{CB})_{mn} \tag{27}$$

containing the contribution of proton transitions to and from the shuttle $\gamma^{\mathrm{tr}}_{mn}(x)$, together with the Marcus rate $(\kappa_{CB})_{mn}$ describing the light-induced electron transfer between the sites B and C,

$$\begin{aligned}(\kappa_{BC})_{mn} = {}& |F_0|^2\sqrt{\frac{\pi}{\lambda_{BC}T}}|(a^\dagger_B a_C)_{mn}|^2 \times\exp\left[-\frac{(\omega_{mn} + \omega_0 + \lambda_{BC})^2}{4\lambda_{BC}T}\right] \\ &+ |F_0|^2\sqrt{\frac{\pi}{\lambda_{BC}T}}|(a^\dagger_B a_C)_{nm}|^2 \times\exp\left[-\frac{(\omega_{mn} - \omega_0 + \lambda_{BC})^2}{4\lambda_{BC}T}\right],\end{aligned} \tag{28}$$

as well as the rates related to the electron transfers between the pairs of sites $(ii') = (DB), (CA), (AS)$, and (DS),

$$(\kappa_{ii'})_{mn} = |\Delta_{i'i}|^2 \sqrt{\frac{\pi}{\lambda_{ii'}T}}[|(a_i^\dagger, a_i)_{mn}|^2 + |(a_{i'}^\dagger, a_i)_{nm}|^2] \times \exp\left[-\frac{(\omega_{mn} + \lambda_{ii'})^2}{4\lambda_{ii'}T}\right]. \quad (29)$$

We note that the tunneling coefficients Δ_{AS} and Δ_{DS} depend on the shuttle position x.

B. Equation of motion for the shuttle

We assume that the shuttle moves along the linear molecular triad (Fig. 1) and this motion can be described by the overdamped Langevin equation for the shuttle position x,

$$\eta_{\text{drag}}\frac{dx}{dt} = -\frac{dU(x)}{dx} + \zeta(t). \quad (30)$$

Here η_{drag} is the drag coefficient of the shuttle in the lipid membrane and the thermal fluctuation of the medium is modeled by a zero-mean delta-correlated Gaussian fluctuation force $\zeta(t)$, $\langle\zeta(t)\rangle = 0$,

$$\langle\zeta(t)\zeta(t')\rangle = 2\eta_{\text{drag}}T\delta(t-t'), \quad (31)$$

where T is the temperature of the medium ($k_B = 1$). The diffusion of the shuttle is determined by the diffusion coefficient $D_s = T/\eta_{\text{drag}}$. The potential $U(x)$ in Eq. (30) is responsible for the spatial confinement of the hydrophobic shuttle (quinone) inside the lipid membrane.

IV. RESULTS AND DISCUSSIONS

To analyze the light-induced proton pumping process quantitatively, we use the standard Heun's algorithm to numerically solve the 20 coupled master equations (26) along with the equation (30) for the shuttle. For initial conditions we have assumed that at $t=0$, $\rho_{1,1}=1$, and the other elements of the density matrix are zero (this corresponds to one electron on site D and another electron on site B with no electrons and no protons on the shuttle). We also assume that at $t=0$ the shuttle is located nearby the acceptor (A): $x(t=0) = x_A \simeq x_N$. Throughout our simulation we focus on the long-term asymptotic regime, where the effects due to the influence of transient processes have been smoothed out. The time-homogeneous statistical properties are obtained in the long-time limit after the temporal and ensemble averaging are performed.

The efficiency (quantum yield) of the proton pumping device is defined by the formula

$$\Phi = \frac{\text{number of protons pumped}}{\text{number of photons absorbed}}.$$

The photon absorption rate $\kappa_{B\to C}$ is approximately equal to the rate of light-induced transitions from the state B to the state C. Thus we assume

$$\Phi \simeq \frac{I_p}{\kappa_{B\to C}}, \quad (32)$$

where I_p is the proton current (the number of protons N_p translocated across the membrane per unit of time).

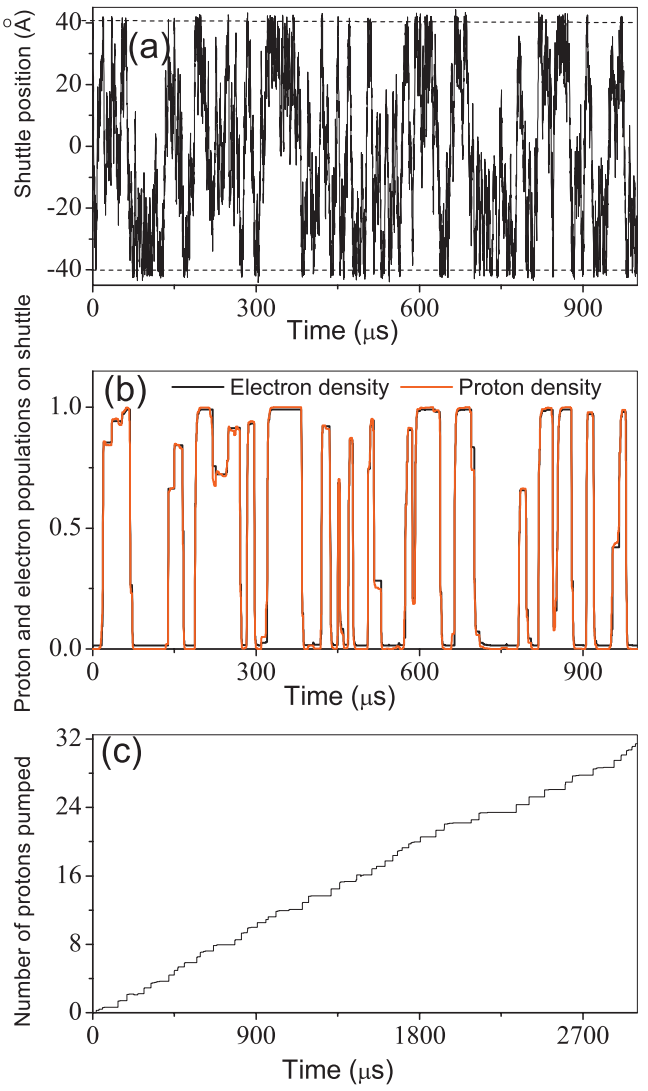

FIG. 5. (a) Stochastic motion of the shuttle with time. The horizontal black dashed lines denote the borders of the membrane $x_N = 40$ Å, $x_P = -40$ Å. Via this diffusion the shuttle transports protons and electrons through the membrane. (b) Variation in the electron and proton population on the shuttle. Note that the proton density (red curve) and the electron density (black curve) mostly coincide in (b). (c) Number of protons pumped vs time. The main parameters used here are the light intensity $I = 0.138$ mW cm^{-2}, temperature $T = 298$ K, and the chemical potentials $\mu_P = 110$ meV and $\mu_N = -110$ meV. The light intensity I corresponds to the photosensitive BC-group with a dipole moment $\sim|e|\times 1$ nm, where e is the electron charge.

A. Diffusive motion of the shuttle in the lipid bilayer

In Fig. 5 we present the diffusive motion [see Fig. 5(a)] of the shuttle in the lipid bilayer together with the time dependencies of the electron and proton populations of the shuttle [Fig. 5(b)] complemented by the time evolution of the number of pumped protons [Fig. 5(c)]. We assume that the reorganization energies for the thermal electron transfers are low enough to provide a high performance of the system

$$\lambda \sim \lambda_{DB} \sim \lambda_{AC} \sim \lambda_{AS} \sim \lambda_{DS} \sim 400 \text{ meV}.$$

This value of λ is quite common for porphyrin-quinone dyads having a lower limit (the internal reorganization energy) of the order of 0.3 eV.[34] Even smaller reorganization energies ($\lambda \sim 230$ meV) have been measured for the porphyrin-

fullerene dyads.[35] The initial stages of electron transfer in bacterial reaction centers[36] are also characterized by a low reorganization energy $\lambda \sim 70-300$ meV depending on the environment. This is due to the fact that the bacteriochlorophyll molecules (and the molecules of porphyrin involved in our molecular triad) contain highly delocalized π-electron systems. In Sec. IV B, we also analyze how sensitive the results are to changes in the values of λ.

Electrochemical measurements[1] show that the energy of the carotene(D)-porphyrin(BC)-quinone(A) molecular triad sweeps from the value of ~1.9 eV (the first excited state of the porphyrin, D-B^1C-A) to the energy of ~1.4 eV related to the intermediate state D-BC^+-A^-, and, finally, to the energy of ~1.1 eV of the charge-separated state D^+-BC-A^-. We assume here that the energy of the first excited state of the porphyrin $E_C - E_B$ is 1908 meV, which corresponds to a photon wavelength of 650 nm as used in experiments.[9,10] We have taken the energy gap between the sites C and A to be approximately equal to the reorganization energy $(E_C - E_A) \sim \lambda = 400$ meV. This gap is about the energy difference between the D-B^1C-A and D-BC^+-A^- states.

The energies of the electron sites S and A are comparable, $(E_A - E_S) \simeq 300$ meV, due to a structural similarity of the quinone shuttle (S) and quinone moiety of the molecular triad. The protonation of the shuttle leads to the lowering of the electron energy on site S due to the electron-proton Coulomb attraction,[9] $u_{SQ} \sim 360$ meV. The other Coulomb interaction terms are chosen as $u_{DB} = u_{BA} = 120$ meV and $u_{DA} = 60$ meV. These values correspond to the electrostatic interaction of two charges located at distances of 4 and 8 nm, respectively (in a medium with a dielectric constant of ~3). Furthermore, we assume that $E_D - E_B = 400$ meV and $\epsilon_Q = 200$ meV. We have chosen ε_Q such that for the above mentioned parameters, the device works well at the transmembrane potential difference of ~200 mV.

We choose $\mu_P = 110$ meV, $\mu_N = -110$ meV, the resonant tunneling rates $\Delta/\hbar = 15$ ns^{-1}, $\Gamma/\hbar = 1.5$ ns^{-1}, and the reorganization energy for the light-induced electron transfer $\lambda_{BC} \sim 80$ meV. The majority of parameters in our model are deduced from experimental data. The rates of electron transfer reactions are given by

$$\kappa_{C\to A} \simeq \kappa_{D\to B} \simeq 26 \ \mu\text{s}^{-1},$$

$$\kappa_{A\to S} \simeq \kappa_{S\to A} \simeq 20 \ \mu\text{s}^{-1}.$$

Therefore, the loading and unloading time scales of the shuttle are about 0.05 μs. The shuttle has enough time to be loaded and unloaded with electrons and protons when it enters the loading/unloading domain with a size of about the electron tunneling length $L_{\text{tun}} \sim 0.5$ nm and the proton transition length $L_Q \sim 0.2$ nm. Figures 5(a) and 5(b) show a time synchronization between the spatial motion of the shuttle and the time variations in the shuttle populations.

It follows from Fig. 5(c) that in 1 ms the shuttle performs near 16 trips and translocates ten protons through the membrane, provided that the light intensity $I = 0.133$ mW cm^{-2}. We assume that the diffusion coefficient D_s is of the order of 2 nm^2 μs^{-1} (Ref. 37) and the dipole moment of the BC moiety is about $|e| \times 1$ nm, where e is the electron charge. The number of photons absorbed in 1 ms is ~18. Thus, the approximate quantum yield Φ of the pumping process is ~55%. For this parameters, the diffusive motion of the shuttle is the slow and rate-limiting step of the pumping process.

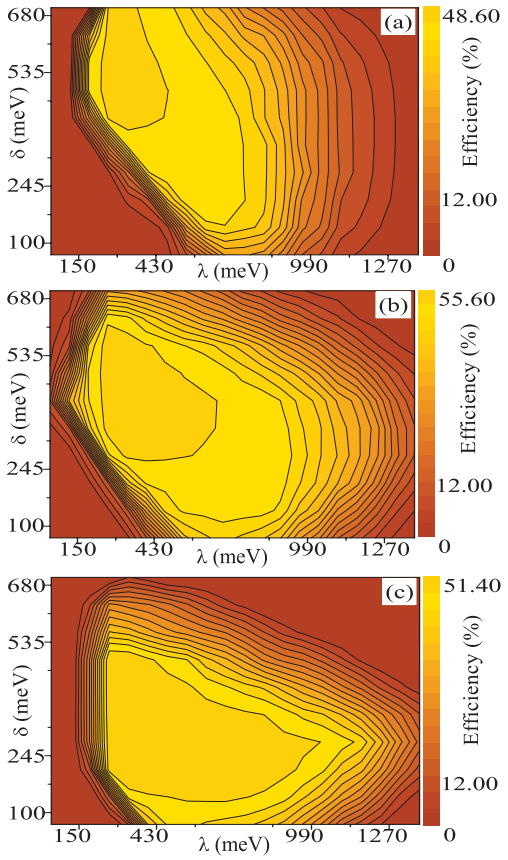

FIG. 6. Contour plots presenting the variations in the quantum efficiency Φ with the reorganization energy λ and with the energy gap δ, where $\delta = E_C - E_A = E_S - E_D$. The parameters used here are light intensity $I = 0.138$ mW cm^{-2}, temperature $T = 298$ K, and chemical potentials $\mu_P = 110$ meV and $\mu_N = -110$ meV. The detunings take the following values: (a) $E_A - E_S = 100$ meV, (b) $E_A - E_S = 300$ meV, and (c) $E_A - E_S = 500$ meV.

B. Robustness of the model

To show a tolerance of the system to variations in parameters we explore here the parameter space of our model. Keeping fixed the energy difference between the sites B and C, we calculate and plot (see Fig. 6) the pumping efficiency Φ (photon-to-proton quantum yield) as a function of the reorganization energy λ and the energy gap δ,

$$\lambda \sim \lambda_{DB} \sim \lambda_{AC} \sim \lambda_{AS} \sim \lambda_{DS},$$

$$\delta = E_C - E_A = E_S - E_D,$$

between the energy levels E_C and E_A, and between the levels E_S and E_D. Figures 6(a)–6(c) correspond to the different values of detuning between the acceptor energy level E_A and the electron energy level on the shuttle E_S: $E_A - E_S = 100$ meV [Fig. 6(a)]; $E_A - E_S = 300$ meV [Fig. 6(b)]; and $E_A - E_S = 500$ meV [Fig. 6(c)]. These plots clearly demonstrate the existence of quite wide areas in the plane $\lambda - \delta$, where the pump performs with maximum efficiency. For the detuning

$E_A - E_S = 100$ meV [Fig. 6(a)] the pumping efficiency reaches its maximum at $\Phi \sim 48\%$ in the region of parameters (in meV): $270 < \lambda < 500$ and $400 < \delta < 700$. In this region, the energy gaps between the redox sites are close to the reorganization energy, which results in higher site-to-site tunneling rates and, consequently, in a high pumping efficiency.

The higher pumping efficiency $\Phi \sim 55\%$ can be achieved at the detuning $E_A - E_S = 300$ meV [Fig. 6(b)]. In this case the parameter δ can be tuned in such a way that the energy gaps between all relevant electron sites are equal to the reorganization energy,

$$(E_C - E_A) \sim (E_A - E_S) \sim (E_S - u_{SQ} - E_D) \sim (E_D - E_B) \sim \lambda.$$

We recall that a shuttle populated with a proton has the electron energy $E_S - u_{SQ}$, which differs from the initial value E_S by the charging energy $u_{SQ} \sim 360$ meV. Summing all the above-mentioned detunings and taking into account the energy difference $E_C - E_B = 1908$ meV between the optically active levels B and C, we estimate the optimum values of the reorganization energy λ and the detuning δ,

$$\lambda \sim \delta \sim (E_C - E_B - u_{SQ})/4 = 387 \text{ meV}.$$

The maximum of the efficiency in Fig. 6(b) is observed at $\delta \sim \lambda \sim 400$ meV, which is very close to our estimations. For a larger energy gap $E_A - E_S = 500$ meV [see Fig. 6(c)], the proton pumping efficiency Φ decreases and the region of the optimum parameters shrinks as compared to Fig. 6(b).

C. Effects of the resonant tunneling rates

The fine tuning of tunneling couplings between active electron sites is feasible in some nanostructures. This tuning can be implemented by changing the site-to-site distance as well as by varying the height of the potential barriers (see, e.g., Ref. 38). Artificial photosynthetic systems such as the molecular triads also allow to engineer desirable tunneling and electrostatic properties of the structures[1] with the goal to achieve the highest possible efficiency. As in colloidal nanocrystals,[38] this can be done by inserting additional molecular bridges between the side centers D, A, and the photosensitive part BC utilizing the exponential dependence of electron tunneling rates on the distance.[5]

In Fig. 7 we illustrate the variation in the proton pumping efficiency Φ as a function of the resonant tunneling rate $(\Delta/\hbar)$ for different values of the reorganization energy λ [Figs. 7(a) and 7(b)] and the energy gap δ [Figs. 7(c) and 7(d)]. The detuning $E_A - E_S$ is fixed to the value of 300 meV for all plots in Fig. 7.

In Fig. 7(a) we plot four curves $\Phi(\Delta)$ for the following set of reorganization energies: $\lambda = 100$, 130, 200, 400 meV and for a detuning $\delta = 400$ meV. In Fig. 7(b) the efficiencies $\Phi(\Delta)$ are plotted for the reorganization energies: $\lambda = 500$, 800, 1000, 1200 meV for the same detuning δ. Similar dependencies $\Phi(\Delta)$ are depicted in Fig. 7(c) for $\delta = 100$, 130, 200, 400 meV and in Fig. 7(d) for $\delta = 500$, 600, 700, 800 meV. In both, Figs. 7(c) and 7(d), the reorganization energy λ is equal to 400 meV.

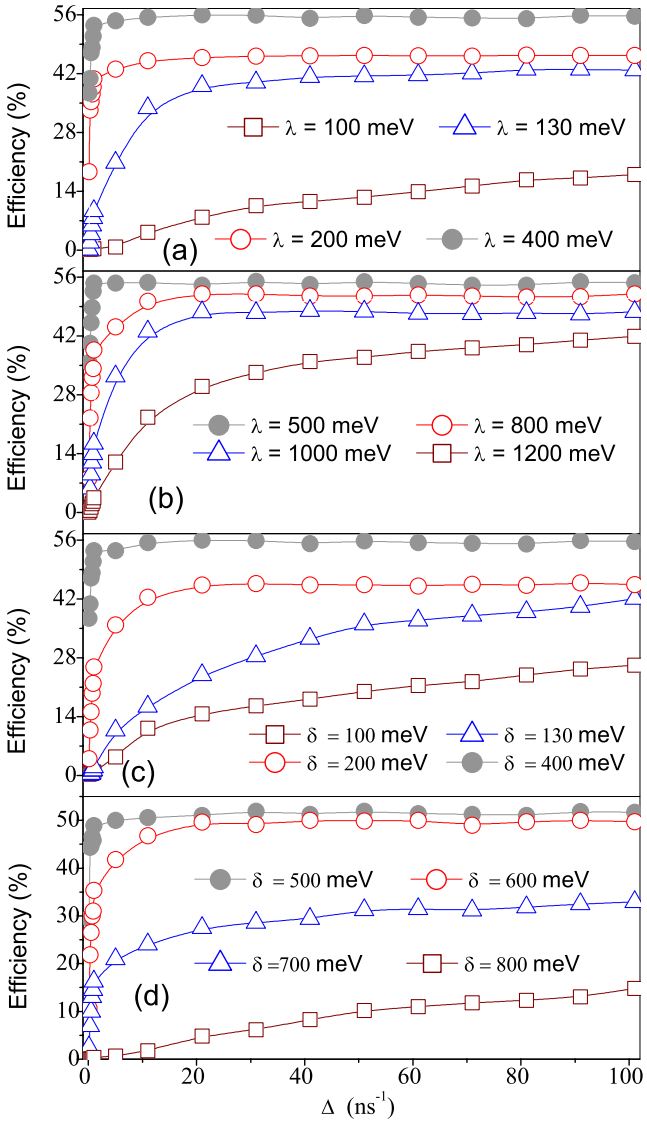

FIG. 7. Proton pumping quantum efficiency Φ vs resonant tunneling rate Δ at different reorganization energies λ shown in (a) and (b) and for different detunings δ shown in (c) and (d). Note that Δ here represents $\Delta/\hbar$ since we set $\hbar = 1$. We use the following parameters: $I = 0.138$ mW cm^{-2}, $T = 298$ K, $\mu_P = 110$ meV, $\mu_N = -110$ meV, and the energy gap $(E_A - E_S) = 300$ meV. Panels (a) and (b) are plotted at fixed $\delta = 400$ meV, whereas in (c) and (d) the reorganization energy is fixed with $\lambda = 400$ meV.

It follows from Fig. 7 that initially the proton pumping efficiency rapidly increases with increasing Δ followed by its saturation for higher values of the resonant tunneling rate. The saturation limit depends on the reorganization energy λ as well as on the energy gap δ. For the optimum values of λ and δ: $\lambda \sim \delta \sim 400$ meV, the pumping efficiency is sufficiently high, $\Phi \sim 55\%$, even for moderate tunneling rates $\Delta/\hbar \leq 5$ ns^{-1}.

D. Effects of Coulomb interactions

In Fig. 8 we plot the efficiency Φ versus the dielectric constant ε of the medium to explore the effects of the Coulomb couplings u_{DB}, u_{BA}, and u_{DA} on the performance of the proton pump. The electrostatic interactions between the photosensitive parts B and C and the donor u_{DB} between the sites B and C and the acceptor u_{BA} and between the donor and the

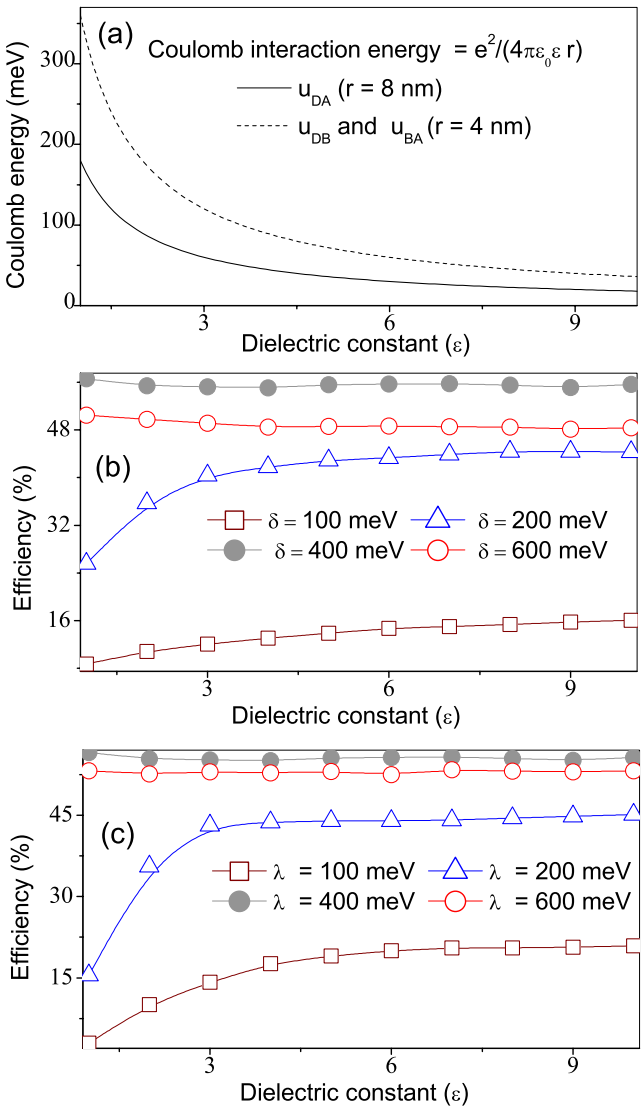

FIG. 8. (a) Coulomb energies u_{DA} and u_{DB} vs the dielectric constant ε of the medium. (b) Proton pumping efficiency Φ vs dielectric constant ε for different values of δ and for λ=400 meV. (c) The pumping efficiency Φ as a function of the dielectric constant ε for different reorganization energies λ and at the fixed detuning δ=400 meV. The other parameters are the same as in Fig. 7: I=0.138 mW cm^{-2}, T=298 K, μ_P=110 meV, μ_N=−110 meV, and $E_A - E_S$=300 meV.

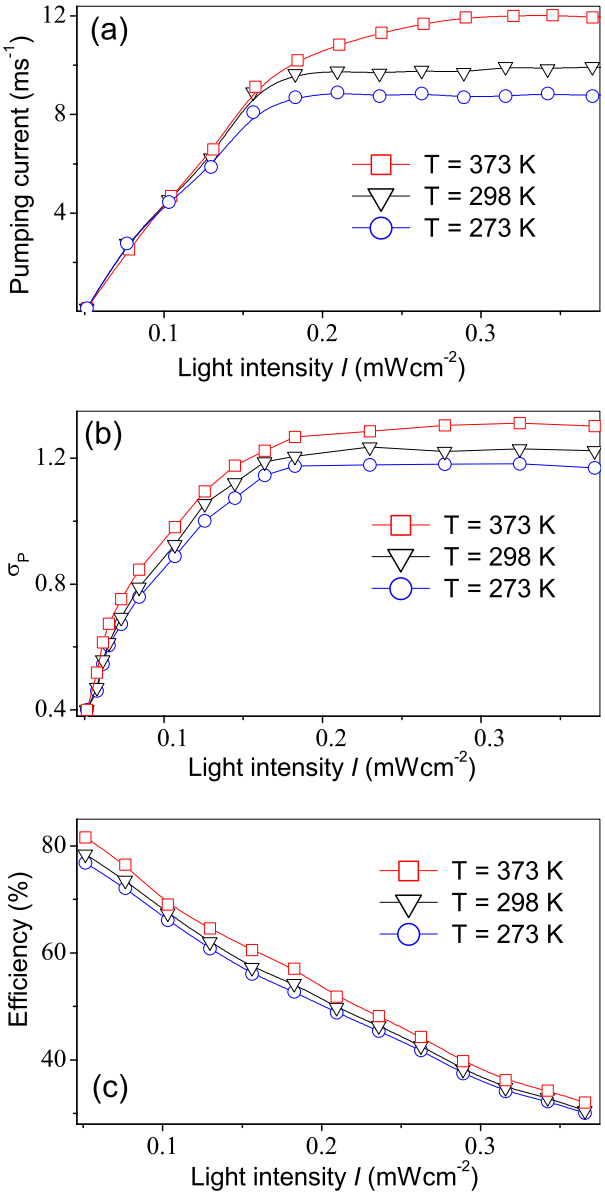

FIG. 9. (a) Proton current vs light intensity I for different temperatures at μ_N=−110 meV and μ_P=110 meV. Notice that the proton current is roughly linear for small intensities of light but it saturates with higher light intensity. In this saturation region, the proton current is larger with higher temperatures. (c) The standard deviation σ_p of the number N_p of pumped protons as a function of the light intensity I for different temperatures. (b) The pumping quantum efficiency Φ decreases with light intensity for all temperatures shown.

acceptor u_{DA} are inversely proportional to the dielectric constant ϵ and to the distance between the relevant sites. For example, we have

$$u_{DB} = \frac{e^2}{4\pi\varepsilon_0 \varepsilon r_{DB}},$$

where r_{DB} characterizes the spatial separation of the sites D and B and ε_0 is the vacuum permittivity. The Coulomb interactions between the sites D and B and between the sites B and A (with $r_{DB}=r_{BA}$=4 nm) are decreased from 360 to 36 meV when the dielectric constant ε scans the range from 1 to 10 [see Fig. 8(a)]. We note that in our model r_{DA}=8 nm, so that $u_{DA}=u_{DB}/2$. Figure 8(b) shows the efficiencies $\Phi(\varepsilon)$ for different values of the detuning δ: δ=100, 200, 400, 600 meV for λ=400 meV. Moreover, in Fig. 8(c) we plot the efficiencies $\Phi(\varepsilon)$ for fixed detuning δ=400 meV and for λ =100, 200, 400, 600 meV.

It should be emphasized that near the optimum working point (at $\lambda \sim \delta \sim 400$ meV) the pump operates with the high efficiency $\Phi \sim 55\%$, which practically does not depend on the dielectric properties of the medium.

E. Effect of light intensity

In Fig. 9 we plot the proton current as a function of the light intensity for different values of the temperature. At zero light intensity the proton current is zero. Initially, with increasing light intensity, the proton current also increases linearly and then saturates around 0.2 mW cm^{-2}. This satura-

tion is probably caused by the slow diffusion of the shuttle inside the lipid membrane. A similar intensity of saturation (~ 0.1 mW/cm^2) has been observed in experiments.[10]

In a warm environment, the shuttle moves faster and carries more protons. To do this, the system should absorb more photons so that at high temperatures a full saturation takes place at higher light intensities. We note that the low saturation limit obtained above and measured in the experiment[10] with the carotene-porphyrin-quinone triads is far below the average intensity of solar light, $I \sim 30$ mW/cm^2.[6] This fact points to the relative inefficiency of the energy-conversion process available at normal daylight conditions. An ideal highly efficient photosynthetic system should not have any saturation limits for the standard daylight intensity of light.

It is evident from Fig. 5 that the number of protons N_p translocated across the membrane fluctuates in time. To estimate these fluctuations we calculate the standard deviation

$$\sigma_p = \sqrt{\langle N_p^2 \rangle - \langle N_p \rangle^2}, \tag{33}$$

which characterizes the magnitude of its shot noise. The dependence of the noise level σ_p on the light intensity I is shown in Fig. 9(b). For an intensity of light $I \sim 0.14$ mW^2/cm^2 (when ~ 10 protons are translocated across the membrane and the efficiency $\Phi \sim 55\%$ is sufficiently high) the uncertainty σ_p in the number of pumped protons is about 1.3. In Fig. 9(c) we demonstrate that the efficiency Φ of the light-induced pumping decreases monotonically with increasing light intensity. At low light intensities, a relatively small number of photons are absorbed per unit time. Thus, a higher fraction of the absorbed photons is used for the uphill pumping of the protons.

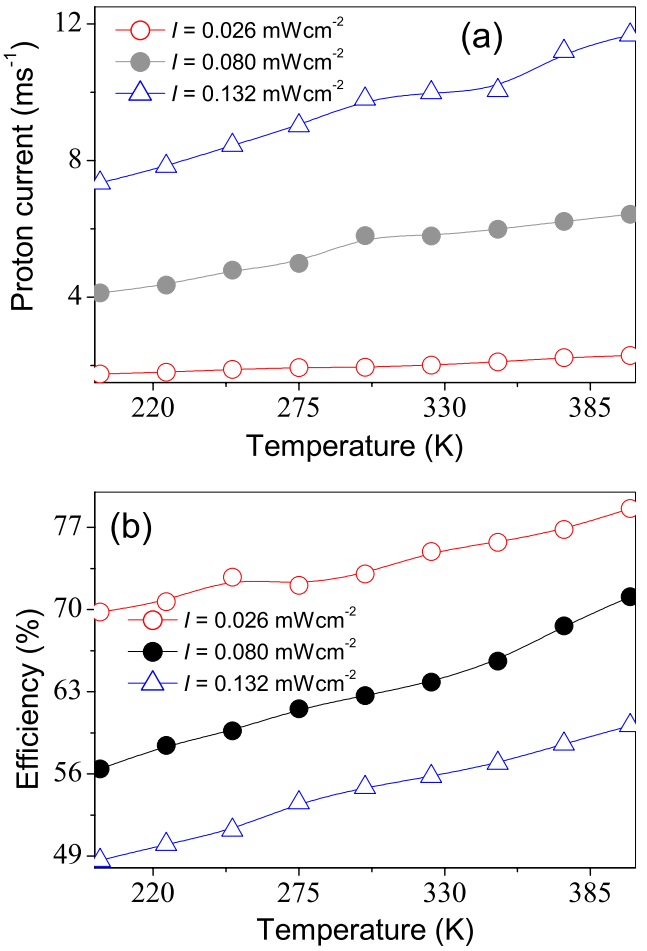

FIG. 10. (a) Proton current vs temperature for different values of the light intensity I. (b) Pumping efficiency Φ vs temperature. Here, the electrochemical gradient $\Delta\mu$=220 meV (μ_P=110 meV and μ_N=−110 meV).

F. Effect of temperature

Figure 10 shows the effects of temperature on the pumping current and on the efficiency of the photosynthetic device for different values of the light intensity. The temperature effects appear in the light-induced proton pumping dynamics through two factors. (i) The electron transfer rates, including the loading and unloading rates of the shuttle, increase with increasing temperature. (ii) The diffusion coefficient of the shuttle increases with temperature. Because of this, the shuttle can perform a higher number of trips to translocate protons at higher temperatures. Here the electron transfer reactions are not rate-limiting ones. The diffusive trips of the shuttle from the N terminal to the P terminal dominate the transfer rate. Therefore, the increase in the efficiency and the pumping current with temperature is due to the increase in the number of diffusive trips of the shuttle. A temperature increase from 200 to 400 K results in an increase of about a factor of 2 in the diffusion constant. It is expected that the proton current should increase at the same rate. However, our calculated ratio is about 1.5 [see Fig. 10(a)]. This is probably due to the fact that at high temperatures the shuttle has not enough time to be completely loaded with electrons and protons near the acceptor site A and the N-side of the membrane (and unloaded near the donor site D and the P-side of the membrane). A similar enhancement of the pumping current and the efficiency with temperature can be useful for photosynthetic microorganisms to compensate a leakage of protons caused by the high-temperature increase in the membrane permeability.[39] The simple physical features which come into play in our model are also important for the creation of thermostable artificial photosynthetic devices efficiently converting energy of light into electrical and chemical energy in a wide range of temperatures and light intensities.

G. Effect of the electrochemical potential gradient on the proton current

It follows from Eq. (14) that the difference $\Delta\mu = \mu_P - \mu_N$ between the electrochemical potentials of P- and N-proton reservoirs can be changed by changing the pH levels of the solutions inside and outside of the liposome. In doing so, one unit change in pH corresponds to ~ 59 meV variation in the transmembrane proton gradient $\Delta\mu$ (at standard conditions). To demonstrate the effect of the pH levels on the performance of the pump, in Fig. 11 we plot the dependencies of the proton current on the electrochemical potential μ_P of the positive side of the membrane at three different values of the N-side potential: $\mu_N = -110$, -140, and -200 meV. The proton current saturates when the P-side potential is sufficiently low, $\mu_P < 160$ meV, and goes to zero

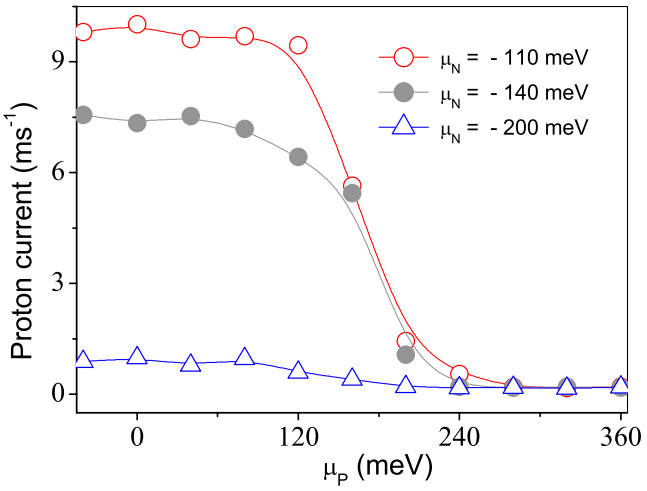

FIG. 11. Proton pumping current vs electrochemical potential μ_P of the positive side (P-reservoir) of the membrane for different values of the potential μ_N of the negative side (N-reservoir) for the light intensity $I=0.132$ mW cm^{-2} and temperature $T=298$ K.

at $\mu_P > 200$ meV. At this condition, the potential of the P-side exceeds the energy $\epsilon_Q = 200$ meV of the proton on the shuttle $\mu_P > \epsilon_Q$, so that the proton cannot be translocated to the P-reservoir. On the other hand, the shuttle cannot be loaded with a proton at the N-side of the membrane if the electrochemical potential μ_N is below the energy $\epsilon_Q - u_{SQ} = -160$ meV of the proton on the shuttle populated with a single electron: $\mu_N < -160$ meV. This is the reason why the last curve in Fig. 11 (taken at $\mu_N = -200$ meV) goes far below the other two curves (plotted for $\mu_N > -160$ meV).

V. CONCLUSIONS

We have analyzed a simple model for light-induced proton pumps in artificial photosynthetic systems. This model has five electron sites [four sites (D,B,C,A) for the triad molecule and one site for the shuttle (S)] and one proton-binding site on the shuttle (Q). The shuttle exhibits diffusive motion in the lipid bilayer, so that the electron and proton populations of the shuttle depend on the shuttle position. Based on the methods of quantum transport theory we have derived and solved numerically a system of master equations for electron and proton state probabilities evolving in time together with the Langevin equation for the position of the shuttle. This allows us to calculate the proton current and the pumping efficiency of the system and determine their dependence on the intensity of light, temperature, and electrochemical potential gradient.

For a reasonable set of parameters closely related to the experimental setup, we demonstrate that this photosynthetic device can translocate protons against an electrochemical gradient of the order of 220 meV with the efficiency (photon-to-proton quantum yield) which exceeds 55%. Our results explain the experiments on artificial photosynthetic reaction centers.[10] We predict that both the proton current and the pumping efficiency grow linearly with temperature due to the related increase in the number of diffusive trips of the shuttle. We also show that the pumping current increases linearly with the light intensity and saturates at the experimentally observed limit, which is lower than the average intensity of solar light.

ACKNOWLEDGMENTS

We acknowledge the partial support from the National Security Agency (NSA), Laboratory for Physical Sciences (LPS), Army Research Office (ARO), and National Science Foundation (NSF) Grant No. EIA-0130383. We also acknowledge the RIKEN Super Combined Cluster System for computational facilities.

APPENDIX: BASIS SETS: ELECTRON-PROTON EIGENSTATES AND ENERGY EIGENVALUES

The electron-proton system studied here with no leads can be characterized by the 20 basis states of the Hamiltonian H_0,

$$
\begin{aligned}
&|1\rangle = a_D^\dagger a_B^\dagger |0\rangle; \quad |11\rangle = a_D^\dagger a_B^\dagger b_Q^\dagger |0\rangle,\\
&|2\rangle = a_D^\dagger a_C^\dagger |0\rangle; \quad |12\rangle = a_D^\dagger a_C^\dagger b_Q^\dagger |0\rangle,\\
&|3\rangle = a_D^\dagger a_A^\dagger |0\rangle; \quad |13\rangle = a_D^\dagger a_A^\dagger b_Q^\dagger |0\rangle,\\
&|4\rangle = a_B^\dagger a_C^\dagger |0\rangle; \quad |14\rangle = a_B^\dagger a_C^\dagger b_Q^\dagger |0\rangle,\\
&|5\rangle = a_B^\dagger a_A^\dagger |0\rangle; \quad |15\rangle = a_B^\dagger a_A^\dagger b_Q^\dagger |0\rangle,\\
&|6\rangle = a_C^\dagger a_A^\dagger |0\rangle; \quad |16\rangle = a_C^\dagger a_A^\dagger b_Q^\dagger |0\rangle,\\
&|7\rangle = a_D^\dagger a_S^\dagger |0\rangle; \quad |17\rangle = a_D^\dagger a_S^\dagger b_Q^\dagger |0\rangle,\\
&|8\rangle = a_B^\dagger a_S^\dagger |0\rangle; \quad |18\rangle = a_B^\dagger a_S^\dagger b_Q^\dagger |0\rangle,\\
&|9\rangle = a_C^\dagger a_S^\dagger |0\rangle; \quad |19\rangle = a_C^\dagger a_S^\dagger b_Q^\dagger |0\rangle,\\
&|10\rangle = a_A^\dagger a_S^\dagger |0\rangle; \quad |20\rangle = a_A^\dagger a_S^\dagger b_Q^\dagger |0\rangle.
\end{aligned}
\tag{A1}
$$

Here, $|0\rangle$ represents the vacuum state when all electron and proton sites are empty. The state $|1\rangle = a_D^\dagger a_B^\dagger |0\rangle$ corresponds to the case when one electron is located on site D, one on site B, and so on. The state $|11\rangle = a_D^\dagger a_B^\dagger b_Q^\dagger |0\rangle$ indicates that in addition to two electrons on sites D and B, there is also a proton on the shuttle. States $|1\rangle$ to $|10\rangle$ describe the shuttle with no protons, whereas states $|11\rangle$ to $|20\rangle$ are related to the shuttle populated with a single proton.

An arbitrary operator A of the combined electron-proton system can be expressed in terms of the basis Heisenberg matrices $\rho_{m,n} = |m\rangle\langle n|$,

$$A = \sum_{m,n} A_{mn} \rho_{m,n},$$

where m and n label the basis states $m,n = 1,\ldots,20$. The diagonal operator is denoted as $\rho_m \equiv \rho_{m,m}$. Thus the electron population operators $\{n_D, n_B, n_C, n_A, n_S\}$ can be represented in the form

$$n_D = \rho_1 + \rho_2 + \rho_3 + \rho_7 + \rho_{11} + \rho_{12} + \rho_{13} + \rho_{17},$$

$$n_B = \rho_1 + \rho_4 + \rho_5 + \rho_8 + \rho_{11} + \rho_{14} + \rho_{15} + \rho_{18},$$

$$n_C = \rho_2 + \rho_4 + \rho_6 + \rho_9 + \rho_{12} + \rho_{14} + \rho_{16} + \rho_{19}, \quad \text{(A2)}$$

$$n_A = \rho_3 + \rho_5 + \rho_6 + \rho_{10} + \rho_{13} + \rho_{15} + \rho_{16} + \rho_{20},$$

$$n_S = \rho_7 + \rho_8 + \rho_9 + \rho_{10} + \rho_{17} + \rho_{18} + \rho_{19} + \rho_{20},$$

and for the operator of the proton population of the shuttle we obtain

$$n_Q = \rho_{11} + \rho_{12} + \rho_{13} + \rho_{14} + \rho_{15} + \rho_{16} + \rho_{17} + \rho_{18} + \rho_{19} + \rho_{20}. \quad \text{(A3)}$$

Using the eigenfunctions [see Eq. (A1)], we can rewrite the Hamiltonian H_0 in a simple diagonal form

$$H_0 = \sum_{m=1}^{20} \varepsilon_m \rho_m \quad \text{(A4)}$$

with the following energy spectrum:

$$\begin{aligned}
&\varepsilon_1 = E_D + E_B; \quad \varepsilon_{11} = \varepsilon_1 + \epsilon_Q \\
&\varepsilon_2 = E_D + E_C; \quad \varepsilon_{12} = \varepsilon_2 + \epsilon_Q, \\
&\varepsilon_3 = E_D + E_A - u_{BA}; \quad \varepsilon_{13} = \varepsilon_3 + \epsilon_Q, \\
&\varepsilon_4 = E_B + E_C - u_{DB}; \quad \varepsilon_{14} = \varepsilon_4 + \epsilon_Q, \\
&\varepsilon_5 = E_B + E_A - u_{DA}; \quad \varepsilon_{15} = \varepsilon_5 + \epsilon_Q, \\
&\varepsilon_6 = E_C + E_A - u_{DA}; \quad \varepsilon_{16} = \varepsilon_6 + \epsilon_Q, \\
&\varepsilon_7 = E_D + E_S; \quad \varepsilon_{17} = \varepsilon_7 + \epsilon_Q - u_{SQ}, \\
&\varepsilon_8 = E_B + E_S; \quad \varepsilon_{18} = \varepsilon_8 + \epsilon_Q - u_{SQ}, \\
&\varepsilon_9 = E_C + E_S; \quad \varepsilon_{19} = \varepsilon_9 + \epsilon_Q - u_{SQ}, \\
&\varepsilon_{10} = E_A + E_S + u_{DB} - u_{BA} - u_{DA}; \quad \varepsilon_{20} = \varepsilon_{10} + \epsilon_Q - u_{SQ}.
\end{aligned} \quad \text{(A5)}$$

The terms $a_i^\dagger a_{i'}$ describing the direct tunneling between all possible coupled sites i and i' are given by the expressions

$$\begin{aligned}
&a_B^\dagger a_D = \rho_{4,2} + \rho_{5,3} + \rho_{8,7} + \rho_{14,12} + \rho_{15,13} + \rho_{18,17}, \\
&a_A^\dagger a_C = \rho_{3,2} + \rho_{5,4} + \rho_{10,9} + \rho_{13,12} + \rho_{15,14} + \rho_{20,19}, \\
&a_B^\dagger a_C = \rho_{1,2} + \rho_{5,6} + \rho_{8,9} + \rho_{11,12} + \rho_{15,16} + \rho_{18,19}, \\
&a_A^\dagger a_S = \rho_{3,7} + \rho_{5,8} + \rho_{6,9} + \rho_{13,17} + \rho_{15,18} + \rho_{16,19}, \\
&a_D^\dagger a_S = -\rho_{1,8} - \rho_{2,9} - \rho_{3,10} - \rho_{11,18} - \rho_{12,19} - \rho_{13,20}.
\end{aligned} \quad \text{(A6)}$$

It should be noted that the operator H_{dir} in Eq. (3) is nondiagonal. The proton operator b_Q can also be expressed in a similar form,

$$b_Q = \sum_{mn} b_{Q,mn} \rho_{m,n}. \quad \text{(A7)}$$

[1] D. Gust and T. A. Moore, Science **244**, 35 (1989).
[2] D. Gust, T. A. Moore, and A. L. Moore, Acc. Chem. Res. **34**, 40 (2001).
[3] G. W. Crabtree and N. S. Lewis, Phys. Today **60**(3), 37 (2007).
[4] D. A. LaVan and J. N. Cha, Proc. Natl. Acad. Sci. U.S.A. **103**, 5251 (2006).
[5] M. R. Wasielewski, J. Org. Chem. **71**, 5051 (2006).
[6] M. Hambourger, G. F. Moore, D. M. Kramer, D. Gust, A. L. Moore, and T. A. Moore, Chem. Soc. Rev. **38**, 25 (2009).
[7] J. Barber, Chem. Soc. Rev. **38**, 185 (2009).
[8] B. Alberts, A. Johnson, J. Lewis, M. Raff, K. Roberts, and P. Walter, *Molecular Biology of the Cell* (Garland Science, New York, 2002), Chap. 14.
[9] G. Steinberg-Yfrach, P. A. Liddell, S. C. Hung, A. L. Moore, D. Gust, and T. A. Moore, Nature (London) **385**, 239 (1997).
[10] G. Steinberg-Yfrach, J. L. Rigaud, E. N. Durantini, A. L. Moore, D. Gust, and T. A. Moore, Nature (London) **392**, 479 (1998).
[11] T. A. Moore, A. L. Moore, and D. Gust, Philos. Trans. R. Soc. London, Ser. B **357**, 1481 (2002).
[12] H. Imahori, Org. Biomol. Chem. **2**, 1425 (2004).
[13] S. Bhosale, A. L. Sisson, P. Talukdar, A. Furstenberg, N. Banerji, E. Vauthey, G. Bollot, J. Mareda, C. Roger, F. Wurthner, N. Sakai, and S. Matile, Science **313**, 84 (2006).
[14] R. E. Palacios, G. Kodis, S. L. Gould, L. de la Garza, A. Brune, D. Gust, T. A. Moore, and A. L. Moore, ChemPhysChem **6**, 2359 (2005).
[15] T. Polivka, M. Pellnor, E. Melo, T. Pascher, V. Sundstrom, A. Osuka, and K. R. Naqvi, J. Phys. Chem. C **111**, 467 (2007).
[16] M. Sykora, K. A. Maxwell, J. M. DeSimone, and T. J. Meyer, Proc. Natl. Acad. Sci. U.S.A. **97**, 7687 (2000).
[17] H. Imahori, J. Phys. Chem. B **108**, 6130 (2004).
[18] S. Saha, A. H. Flood, J. F. Stoddart, S. Impellizzeri, S. Silvi, M. Venturi, and A. Credi, J. Am. Chem. Soc. **129**, 12159 (2007).
[19] A. C. Rizzi, M. van Gastel, P. A. Liddell, R. E. Palacios, G. F. Moore, G. Kodis, A. L. Moore, T. A. Moore, D. Gust, and S. E. Braslavsky, J. Phys. Chem. A **112**, 4215 (2008).
[20] H. Imahori, Y. Mori, and Y. Matano, J. Photochem. Photobiol., B **4**, 51 (2003).
[21] J. A. Soderhall and A. Laaksonen, J. Phys. Chem. B **105**, 9308 (2001).
[22] L. Cristian, P. Piotrowiak, and R. S. Farid, J. Am. Chem. Soc. **125**, 11814 (2003).
[23] A. Okada and T. Bandyopadhyay, J. Chem. Phys. **111**, 1137 (1999).
[24] A. Parusel, J. Mol. Model. **4**, 366 (1998).
[25] N. S. Wingreen, A. P. Jauho, and Y. Meir, Phys. Rev. B **48**, 8487 (1993).
[26] A. Yu. Smirnov, L. G. Mourokh, and F. Nori, Phys. Rev. E **77**, 011919 (2008).
[27] A. Yu. Smirnov, S. Savel'ev, L. G. Mourokh, and F. Nori, Phys. Rev. E **78**, 031921 (2008).
[28] A. Yu. Smirnov, L. G. Mourokh, and F. Nori, J. Chem. Phys. **130**, 235105 (2009).
[29] R. A. Marcus and N. Sutin, Biochim. Biophys. Acta **811**, 265 (1985).
[30] D. A. Cherepanov, L. I. Krishtalik, and A. Y. Mulkidjanian, Biophys. J. **80**, 1033 (2001).
[31] H. Imahori, H. Yamada, D. M. Guldi, Y. Endo, A. Shimomura, S. Kundu, K. Yamada, T. Okada, Y. Sakata, and S. Fukuzumi, Angew. Chem., Int. Ed. **41**, 2344 (2002).
[32] J. Y. Kim, K. Lee, N. E. Coates, D. Moses, T.-Q. Nguen, M. Dante, and A. J. Heeger, Science **317**, 222 (2007).
[33] A. Garg, J. N. Onuchic, and V. Ambegaokar, J. Chem. Phys. **83**, 4491 (1985).
[34] H. Heitele, F. Pöllinger, T. Häberle, M. E. Michel-Beyerle, and H. A. Staab, J. Phys. Chem. **98**, 7402 (1994).
[35] H. Imahori, N. V. Tkachenko, V. Vehmanen, K. Tamaki, H. Lemmetyinen, Y. Sakata, and S. Fukuzumi, J. Phys. Chem. A **105**, 1750 (2001).
[36] W. W. Parson, Z. T. Chu, and A. Warshel, Biophys. J. **74**, 182 (1998).
[37] T. Geyer and V. Helms, Biophys. J. **91**, 927 (2006).
[38] D. J. Milliron, S. M. Hughes, Y. Cui, L. Manna, J. Li, L.-W. Wang, and A. P. Alivisatos, Nature (London) **430**, 190 (2004).
[39] J. L. C. M. van de Vossenberg, T. Ubbink-Kok, M. G. L. Elferink, A. J. M. Driessen, and W. N. Konings, Mol. Microbiol. **18**, 925 (1995).